



# Frequency comb dynamics of a 13 $\mu\text{m}$ hybrid-silicon quantum dot semiconductor laser with optical injection

Raymond G Beausoleil, Frédéric Grillot, Bozhang Dong, Heming Huang,  
Jianan Duan, Geza Kurczveil, Di I Liang

## ► To cite this version:

Raymond G Beausoleil, Frédéric Grillot, Bozhang Dong, Heming Huang, Jianan Duan, et al.. Frequency comb dynamics of a 13  $\mu\text{m}$  hybrid-silicon quantum dot semiconductor laser with optical injection. Optics Letters, 2019, 44 (23), pp.5755. 10.1364/OL.44.005755 . hal-02437870

**HAL Id: hal-02437870**

**<https://telecom-paris.hal.science/hal-02437870>**

Submitted on 17 Jan 2020

**HAL** is a multi-disciplinary open access archive for the deposit and dissemination of scientific research documents, whether they are published or not. The documents may come from teaching and research institutions in France or abroad, or from public or private research centers.

L'archive ouverte pluridisciplinaire **HAL**, est destinée au dépôt et à la diffusion de documents scientifiques de niveau recherche, publiés ou non, émanant des établissements d'enseignement et de recherche français ou étrangers, des laboratoires publics ou privés.

# Frequency comb dynamics of a 13 $\mu\text{m}$ hybrid-silicon quantum dot semiconductor laser with optical injection

Bozhang Dong, Heming Huang, Jianan Duan, Geza Kurczveil, Di Liang,  
Raymond Beausoleil, Frédéric Grillot

## ► To cite this version:

Bozhang Dong, Heming Huang, Jianan Duan, Geza Kurczveil, Di Liang, et al.. Frequency comb dynamics of a 13  $\mu\text{m}$  hybrid-silicon quantum dot semiconductor laser with optical injection. Optics Letters, Optical Society of America, 2019, 44 (23), pp.5755. 10.1364/OL.44.005755 . hal-02437870

**HAL Id: hal-02437870**

**<https://hal.telecom-paristech.fr/hal-02437870>**

Submitted on 17 Jan 2020

**HAL** is a multi-disciplinary open access archive for the deposit and dissemination of scientific research documents, whether they are published or not. The documents may come from teaching and research institutions in France or abroad, or from public or private research centers.

L'archive ouverte pluridisciplinaire **HAL**, est destinée au dépôt et à la diffusion de documents scientifiques de niveau recherche, publiés ou non, émanant des établissements d'enseignement et de recherche français ou étrangers, des laboratoires publics ou privés.

# Frequency comb dynamics of a 1.3- $\mu\text{m}$ hybrid-silicon quantum dot semiconductor laser with optical injection

BOZHANG DONG<sup>1,\*</sup>, HEMING HUANG<sup>1</sup>, JIANAN DUAN<sup>1</sup>, GEZA KURCZVEIL<sup>2</sup>, DI LIANG<sup>2</sup>, RAYMOND G. BEAUSOLEIL<sup>2</sup>, AND FRÉDÉRIC GRILLOT<sup>1,3</sup>

<sup>1</sup>LTCI, Télécom Paris, Institut Polytechnique de Paris, 46 rue Barrault, 75013 Paris, France

<sup>2</sup>Hewlett Packard Labs, 1501 Page Mill Road, Palo Alto, CA 94304, USA

<sup>3</sup>Center for High Technology Materials, University of New-Mexico, 1313 Goddard St SE, Albuquerque, New-Mexico 87106, USA

\*Corresponding author: bozhang.dong@telecom-paris.fr

Compiled January 17, 2020

This work reports on the influence of bias voltage applied on saturable absorber (SA) on sub-threshold linewidth enhancement factor (LEF) in hybrid-silicon quantum dot optical frequency comb lasers (QD-OFCs). Results show that the reverse bias voltage on SA contributes to enlarge the LEF and improve the comb dynamics. Optical injection is also found to be able to improve the comb spectrum in term of 3-dB bandwidth and its flatness. Such novel findings are promising for the development of high-speed dense wavelength division multiplexing (DWDM) photonic integrated circuits (PICs) in optical interconnects and datacom applications.

<http://dx.doi.org/10.1364/ao.XX.XXXXXX>

Wavelength-division multiplexing (WDM) solutions can be strongly supported by a variety of photonics integrated technologies that can be reused as what was done in telecommunication industry in using the vast amount of bandwidth offered by optical fibers which contributed to enhance the data transmission. Therefore, the largest future cost reduction due to integration will then likely be enjoyed by more feature-rich blocks such as WDM versus single-wavelength interface[1]. The realization of WDM functions is mainly based on the multiple single-wavelength laser sources, however, the massive laser bar could be disadvantage in several applications such as photonic integrated circuits (PICs). Optical frequency combs (OFCs) are thus a competitive candidate for WDM, considering that the past laser bar could be easily replaced by a single laser. Various researches on OFCs were deployed in the past decade for optical communications in particular with quantum dot (QD) lasers which were found to be efficient comb light sources owing to the very large gain bandwidth[2] as well as to the narrow linewidth[2, 3], low relative intensity noise[4] and higher resistance against external reflections[5, 6] and temperature[7]. With the view of developing low-cost and energy-efficient integrated photonic components for PIC technologies, hybrid semiconductor comb lasers fabricated on silicon substrate have already shown high transmission efficiency[8]. Further improvements need to be

carefully taken into account so as to obtain high performance OFCs with much larger bandwidth and optimal comb flatness. To this end, various techniques such as phase-modulation[9], mode-locking[10, 11] and optical injection-locking (OIL)[12, 13] have been deployed. In this Letter, one goes a step beyond by investigating the effects of the linewidth enhancement factor (LEF) and the optical injection (OI) on the comb performance of hybrid-silicon QD-OFCs. The former is known to be a key parameter in semiconductor lasers hence influencing the spectral linewidth and the frequency chirp under direct modulation [14]. On the other hand, OI was proved to be an efficient way of improving the performance of semiconductor lasers such as the modulation bandwidth, the frequency chirp as well as the intensity noise, and the transmission efficiency[15–17]. In this Letter, it is also shown that the frequency comb dynamics is stimulated at larger LEFs whereas the optical injection can further improve both the bandwidth and the flatness of the entire comb spectrum. To do so, we report on the saturable absorber (SA) voltage dependence of the LEFs extracted from two hybrid-silicon QD-OFCs (named *L1* and *L2*) and having the same free spectral range (FSR). The values of the LEFs are found to increase with the SA reverse voltage which is in favor of a better comb dynamics through increasing the single-mode suppression ratio (SMSR) of the comb lines. Last but not the least, the observed enhancement of both the bandwidth and the flatness of the entire comb spectrum proves that the OI technique is also strongly beneficial for improving the OFCs dynamics.

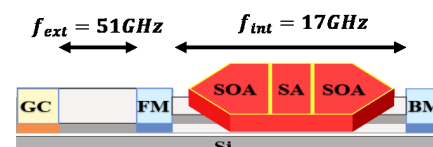


**Fig. 1.** Schematic diagram of the hybrid-silicon QD-OFCs *L1*. SOA, semiconductor optical amplifier; SA, saturable absorber; BM, back mirror; FM, front mirror; GC, grating coupler.

Figure 1 depicts the schematic diagram of the hybrid-silicon QD-OFCs *L1*, the full laser epitaxial structure could be found elsewhere[8]. Device *L1* consists of a 2.3-mm-long internal cavity

which leads to 17 GHz FSR. A 1200- $\mu\text{m}$ -long semiconductor optical amplifier (SOA) with a 120- $\mu\text{m}$ -long SA at the center were then bonded on the laser cavity, with front mirror (FM) and back mirror (BM) at  $\sim 50\%$  and  $\sim 100\%$  power reflectivities placed at both sides. The 0.75-mm-long (51 GHz) external cavity placed outside the laser cavity is then applied to get a 102 GHz FSR on frequency comb behavior. To do so, the SA at the center contributes at first to suppress every even mode of the laser cavity, thus changing the FSR from 17 GHz to 34 GHz; then, the 51 GHz external cavity would only transmit every third mode of the 34 GHz FSR, and eventually ensures that the channel spacing of the comb laser equal to 102 GHz ( $6^{\text{th}}$  harmonic of 17 GHz). The light would finally coupled out by a  $\sim 10\%$  coupling efficiency grating coupler (GC). The comb dynamics is observed by varying the reverse voltage applied on the SA whereas the mode converters are applied to transfer the optical mode between the active hybrid waveguide and the passive Si waveguide. Compared to L1, the differences in L2 structure are that it has not only a wider silicon waveguide of 0.85- $\mu\text{m}$  (compared to 0.68- $\mu\text{m}$  on device L1) but also a shorter SA of 60- $\mu\text{m}$ . As those features may eventually cause a degradation in the OFCs performance, the experimental study depicted hereinafter is mainly performed with device L1. In what follows, measurements are all conducted at room temperature (293 K)

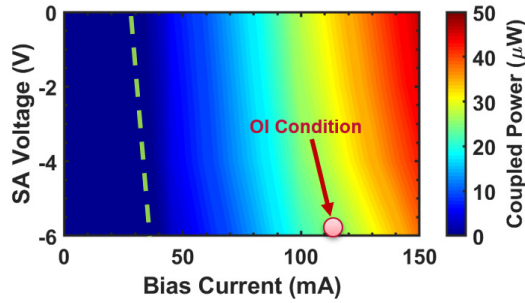


**Fig. 2.** Mapping of the coupled power (QD-OFCs L1) under different reverse voltage on SA and bias current conditions. The green dashed line represents the evolution of the laser threshold with the reverse voltage. The red bullet corresponds to the device operation conditions applied in the optical injection (OI), which is introduced in this paper hereafter.

Figure 2 depicts a mapping of the coupled power of L1 for different reverse voltage on SA and bias current conditions. The evolution of the threshold current  $I_{th}$  marked by the green dashed line is found to slightly increase from 32 to 38 mA as the reverse voltage is varied from 0V to -6V. At the same time, the coupled output power also decreases at higher reverse voltages. Such phenomenon, similar to that observed in mode-locked QD lasers on silicon[18], is due to the higher internal loss caused from the larger absorption in the SA. Let us note that the coupled power remains pretty low due to the loss induced by the vertical grating and the difficulty to monitor the coupling during the whole experiment. A similar trend could also be observed on device L2 (not shown here).

Then, the effects of SA reverse voltage and bias current from the gain section on the combs dynamics are shown in Figure 3 (device QD-OFCs L1). As aforementioned, the contribution of the SA on the occurrence of the comb dynamics can be clearly seen. Without biasing the SA, no comb spectrum is observed (Fig.3(a)) whereas under a reverse voltage of -6V, the laser ex-

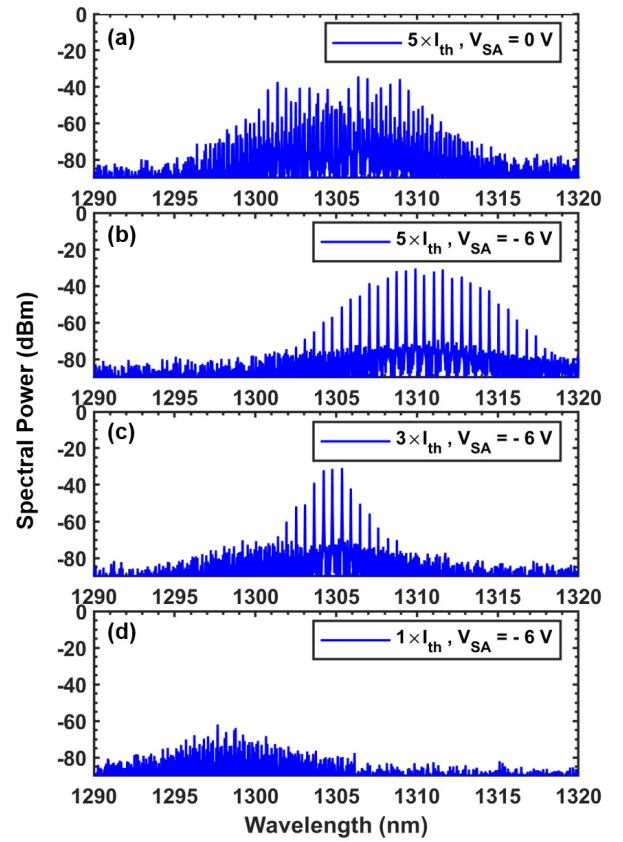
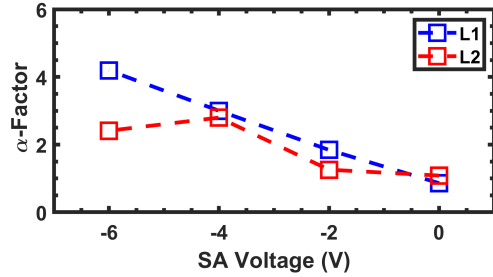


**Fig. 3.** Optical spectrum of QD-OFCs L1 at (a)  $5 \times I_{th}$  without biasing SA and evolution of the combs forms of QD-OFCs L1 under bias voltage at -6V on SA, with bias current at (b)  $5 \times I_{th}$ , at (c)  $3 \times I_{th}$  and at (d)  $1 \times I_{th}$ .

hibits a clear comb spectrum (Fig.3(b)) at  $5 \times I_{th}$ . On the other hand, frequency comb behavior appear when the SA is properly biased, and the central wavelength red-shift results from the increased internal loss introduced by absorption effect from SA as well. Assuming the best comb performance with -6V reverse voltage, the influence of the bias current on the combs dynamics is now displayed in Fig.3(b)-(d). The increase of the bias current from  $1 \times I_{th}$  to  $5 \times I_{th}$  leads to a shift of the central frequency comb from 1298 nm to 1312 nm. This red-shift of the comb position with the bias current is due to thermal effects. Moreover, it should be noticed that both the bandwidth and the flatness of the comb spectrum are also enhanced with the bias current. At  $3 \times I_{th}$ , the comb spectrum exhibits 12 lines above noise floor and 3 lines within 3 dB bandwidth (Fig.3(c)) against 26 and 8 respectively when the bias current increases to  $5 \times I_{th}$  (Fig.3(b)). In general, comb dynamics is usually explained through four-wave mixing (FWM) effect that is ruled out by the LEF[19]. In particular, both the sign and amplitude of the LEF associated to the different individual processes determine how the corresponding third-order susceptibilities contributions add up [20]. By the way, with the devices under study, a continuous-wave (CW) output, containing no pulses, is preferred for WDM applications as such devices are likely to have better reliability from the lower instantaneous power. In addition, the high instantaneous power of a temporally mode-locked laser is likely to trigger unwanted thermal non-linearities[21] in the microring modulator array

which would degrade the signal being transmitted.

In this section, the extraction of the LEF is performed from the amplified spontaneous emission (ASE)[5, 22]. In the experiment, we used a CW current source to get smooth optical modes, which would then be captured by a 20 pm high resolution optical spectrum analyzer (OSA). Such operation ensures a better precision of the LEF extraction. The modal wavelength red-shift above threshold caused by thermal effects is then totally subtracted from the wavelength blue-shift below threshold, hence leading to an accurate extraction of the LEF from below to threshold. Let us note that the device temperature is carefully monitored and kept constant at room temperature (293K) throughout the experiment.



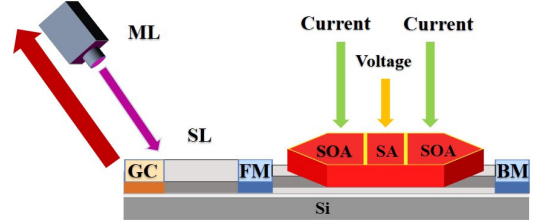
**Fig. 4.** The measured LEF at threshold as the function of the reverse voltage on SA for the QD-OFCs L1 (blue) and L2 (red).

Figure 4 displays the extracted LEF values (threshold) as the function of the reverse voltage on SA for devices L1 (blue) and L2 (red). In both cases, the LEFs are found to increase with the reverse voltage due to the decrease of the differential gain. For instance, it varies from 0.9 (without reverse voltage on SA) to 4.2 (-6V on SA) for device L1. As for L2, a similar trend is observed except at the highest reverse voltage for which the LEF slightly drops down to 2.4. This last effect is attributed to the higher bias voltage applied on a shorter SA causing more carriers being swept-out and leading to a stronger reduction of the stimulated photon density. Together these assumptions can explain the redecree of the LEF at -6V for device L2. Experiments depicted in Fig.3 show that the comb dynamics is optimal when the LEF is larger. **Indeed, the effective LEF  $\alpha_e$  can be calculated from the quadratic mean by integrating over the entire comb spectrum such as,**

$$\alpha_e = \sqrt{\frac{1}{\Delta\nu} \int_{comb} d\nu' \alpha^2(\nu')} \quad (1)$$

with  $\Delta\nu$  the width of the comb spectrum while  $\nu$  is the frequency of the radiation emitted by the laser. Therefore, assuming a QD as a two-level atomic system and that the entire gain media of the QD laser is composed of uniform QD with the same size, integration of (1) leads to  $\Delta\nu = 2\sqrt{3}\Gamma\alpha_e$  with  $\Gamma$  the homogeneous broadening of the QD transition. **Let us stress that this relationship is obtained assuming that the center of the emitted comb spectrum corresponds to the center of the QD transition.** Thus, this equation shows that a larger LEF is indeed more beneficial for improving the comb dynamics through FWM as shown in Fig.3 [23]. A larger LEF was also proved to enhance the mode-locking effect [24], which is in favor of improving the frequency comb dynamics. On the top of that, this equation shows that strengthening the spatial overlap among the dots hence increasing the temperature-dependent homogeneous broadening can a priori contribute to further broaden the comb bandwidth[25].

However, this last statement has some limitations since the increase of the inhomogeneous broadening will not necessary lead to an unlimited increase of the frequency comb bandwidth. Indeed, for larger gain linewidth, the FWM that is intended as self-injection locking mechanism, in providing equally spaced and phase-locked modes becomes less efficient because the dispersion for high frequency active modes is bigger. Also, it is important to remind that the inhomogeneous broadening remains fundamentally an incoherent mechanism thus potentially being more detrimental for a coherent phenomenon like frequency combs.



**Fig. 5.** Schematic illustrating optical injection operation. ML, master laser; SL, slave laser.

As aforementioned, OIL has been broadly used in semiconductor lasers with the view to enhance the relaxation oscillations, or to reduce the relative intensity-to-noise, the nonlinear distortion, and most importantly the linewidth and frequency chirp [15]. In this Letter, we also investigated the effects of the OI as a way to process optical frequency comb by isolating and amplifying individual comb modes. A schematic illustrating the experimental setup is represented in Figure 5. To this end, a master laser (ML) and a slave laser (SL) are involved. The master laser is a single-mode laser with a narrow spectral linewidth which is injected into the slave comb QD laser. The injection strength  $R_{inj}$ , in dBm, is calculated through the relationship:

$$R_{inj} = P_{ml} - P_{out} + 2 \times (L_{ext} + L_{fm} + L_{gc}) \quad (2)$$

where  $P_{ml}$  the injection power of ML,  $P_{out}$  the free-space output power of the SL,  $L_{ext}$  the one-way external cavity waveguide loss,  $L_{fm}$  and  $L_{gc}$  are the FM and GC transmission loss respectively. In the experiments, the values of  $L_{fm}$  and  $L_{gc}$  could be confirmed at -3dB and -9dB respectively. By the way, the waveguide loss  $L_{ext}$  structures were not present on the mask but it is estimated to be less than 2 dB/mm based on data from previous process runs. This should give an upper limit on the loss of the external cavity. Taking  $L_{ext}$  into account, the total loss could exceed -12dB. Nevertheless, when it comes to the calculation of  $R_{inj}$ , such loss introduced by the external cavity should be doubled and eventually would exceed -24dB.

Let us note that in these experiments, the frequency of the slave QD comb laser is not locked to that of the master laser. Instead, a low OI strength is considered in order to optimize the combs dynamics. OI operation is served when the device L1 works at  $3 \times I_{th}$  with -6V applied on SA, the  $R_{inj}$  could thus be estimated to be below -12 dB based on equation 2, as the  $P_{ml}$  and  $P_{out}$  are found to be 6 dBm and -6 dBm respectively. Due to such low injection strength, the LEF is considered not being affected by the injected field. In other words, the LEF can be treated as a constant and does not impact the changes observed in the comb dynamics. Figure 6 unveils two types OI-driven states on device L1 when operated at  $3 \times I_{th}$  with -6V reverse voltage on the SA.



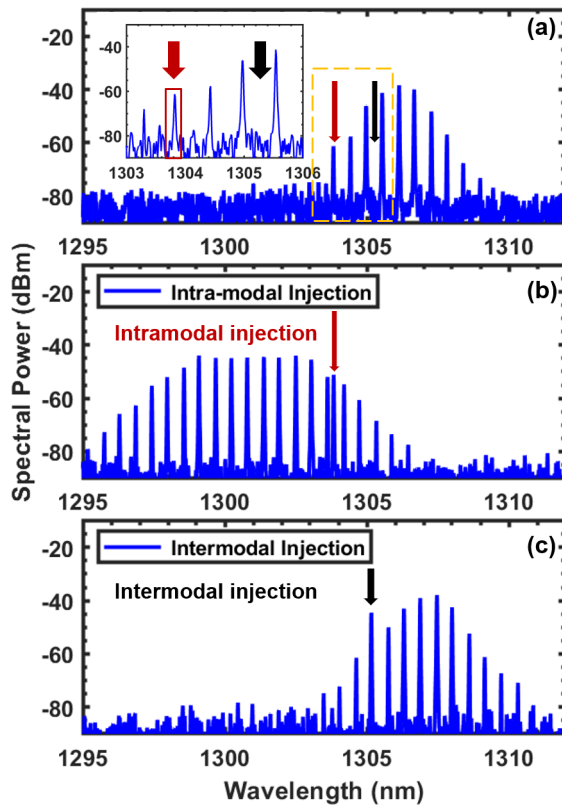


**Fig. 6.** (a) Optical spectra of L1 at free-running, and in inset, the magnification of the yellow area in the figure. The intramodal injected wavelength (red arrow) and the intermodal injection wavelength (black arrow) of ML are highlighted. Optical spectra of L1 (b) under intramodal optical injection at 1303.9 nm (red arrow) and (c) under intermodal optical injection at 1305.2 nm (black arrow). Device is operated at  $3 \times I_{th}$  and bias voltage applied on SA equals to -6V.

The free-running state (without OI) is shown in Fig. 6(a) as a reference. The inset of Fig. 6(a) highlights the injection wavelength of ML, seeing that the intramodal injection and intermodal injection are marked by a red arrow and a black arrow respectively. Once OI intramodal injection is applied (injection wavelength at 1303.9 nm in this case, marked by a red arrow in Fig. 6(b)), a blue-shift of the comb spectrum is observed. In this configuration, both the bandwidth and flatness of the comb spectrum can be regenerated compared to the free-running state. For instance, the full bandwidth of the comb laser broadens from 5.7 nm (11 lines above noise floor) to 10.7 nm (20 lines above noise floor), and its 3-dB bandwidth enlarges from 1.1 nm (3 lines) to 4 nm (8 lines).

On the other hand, another OI-driven state can also be observed when intermodal OI is applied with an injection wavelength at 1305.2 nm as marked by black arrow in Fig. 6(c). However, in this configuration, no obvious improvements of the comb dynamics is observed despite a slight red-shift of the comb central wavelength. Therefore, intermodal injection does not allow to improve neither the bandwidth nor the flatness of the entire comb spectrum. The reasons why two OI-driven states are unveiled between intra and intermodal injections are uncertain yet, hence corresponding studies would be investigated in

further work.

To summarize, this work demonstrates the influence of the SA reverse voltage on sub-threshold LEFs of hybrid-silicon QD-OFCs as well as the optical injection effect on enhancing the bandwidth and flatness of OFCs. Larger LEF was observed when higher reverse voltage was applied on SA, which contributes to enhance OFCs performance. Intramodal OI was shown to improve the bandwidth and flatness of the comb spectrum. Those novel findings are very encouraging for the future integrated technologies required for optical interconnects and datacom applications. Further work will now concentrate on the improvement of the QD devices as well as on the loss reduction in the experimental set-up.

**Disclosures.** The authors declare no conflicts of interest.

## REFERENCES

1. L. Han, B. P.-P. Kuo, N. Alic and S. Radic, Opt. Fiber Commun. Conf. Exhib. (OFC) pp. 1–3 (2019).
2. Z. G. Lu, J. R. Liu, C. Y. Song, J. Weber, Y. Mao, S. D. Chang, H. P. Ding, P. J. Poole, P. J. Barrios, D. Poitras, S. Janz and M. O'Sullivan, Opt. Express **26**, 2160 (2018).
3. J. Duan, H. Huang, Z. G. Lu, P. J. Poole, C. Wang and F. Grillot, Appl. Phys. Lett. **112** (2018).
4. G. L. Wojcik, D. Yin, A. R. Kovsh, A. E. Gubenko, I. L. Krestnikov, S. S. Mikhlin, D. A. Livshits, D. A. Fattal, M. Fiorentino and R. G. Beausoleil, Proc **7230** (2009).
5. J. Duan, H. Huang, B. Dong, D. Jung, J. C. Norman, J. E. Bowers and F. Grillot, IEEE Photonics Technol. Lett. **31** (2019).
6. A. Liu, T. Komljenovic, M. Davenport, A. Gossard and J. Bowers, Opt. Express **25**, 9535 (2017).
7. T. Kageyama, K. Nishi, M. Yamaguchi, R. Mochida, Y. Maeda, K. Takemasa, Y. Tanaka, T. Yamamoto, M. Sugawara and Y. Arakawa, CLEO-Europe (2011).
8. G. Kurczveil, M. A. Seyedi, D. Liang, M. Fiorentino and R. G. Beausoleil, IEEE Photonics Technol. Lett. **30** (2018).
9. V. R. Supradeepa and A. M. Weiner, Opt. Lett. **37** (2012).
10. Z.G. Lu, J.R. Liu, P.J. Poole, S. Raymond, P.J. Barrios, D. Poitras, G. Pakulski, P. Grant and D. Roy-Guay, Opt. Express **17** (2009).
11. M. Yu, Y. Okawachi, A. G. Griffith, M. Lipson and A. L. Gaeta, Optica **3** (2016).
12. E. Sooudi, C. de Dios, J. G. McInerney, G. Huyet, F. Lelarge, K. Merghem, R. Rosales, A. Martinez, A. Ramdane and S. P. Hegarty, IEEE J. Sel. Top. Quantum Electron. **19** (2013).
13. E. Prior, C. De Dios, R. Criado, M. Ortsiefer, P. Meissner and P. Acedo, Opt. Lett. **41** (2016).
14. F. Grillot, B. Dagens, J. G. Provost, H. Su and L. F. Lester, IEEE J. Quantum Electron. **44**, 946 (2008).
15. E. K. Lau, L. J. Wong and M. C. Wu, IEEE J. Sel. Top. Quantum Electron. **15** (2009).
16. N. A. Naderi, M. Pochet, F. Grillot, N. B. Terry, V. Kovanis and L. F. Lester, IEEE J. Sel. Top. Quantum Electron. **15**, 563 (2009).
17. J. Jignesh, A. Lowery and B. Corcoran, Opt. Express **26** (2018).
18. S. Liu, X. Wu, D. Jung, J. C. Norman, M. J. Kennedy, H. K. Tsang, A. C. Gossard and J. E. Bowers, Optica **6**, 128 (2019).
19. T. Akiyama, H. Kuwatsuka, N. Hatori, Y. Nakata, H. Ebe and M. Sugawara, IEEE Photonics Technol. Lett. **14**, 1139 (2002).
20. Govind P. Agrawal, J. Opt. Soc. Am. B **5**, 147 (1988).
21. M. De Cea, A. H. Atabaki and R. J. Ram, Opt. Express **27**, 24274 (2019).
22. M. Osinski and J. Buus, IEEE J. Quantum Electron. **23**, 9 (1987).
23. F. Cappelli, G. Villares, S. Riedi and J. Faist, Optica. **2**, 836 (2015).
24. M. Heuck, S. Blaaberg and J. Mørk, Opt. Express **18** (2010).
25. F. Grillot, K. Veselinov, M. Gioannini, I. Montrosset, J. Even, R. Piron, E. Homeyer and S. Lualich, IEEE J. Quantum Electron. **45**, 872 (2009).

## FULL REFERENCES

1. L. Han, B. P.-P. Kuo, N. Alic and S. Radic, *Opt. Fiber Commun. Conf. Exhib. (OFC)* pp. 1–3 (2019).
2. Z. G. Lu, J. R. Liu, C. Y. Song, J. Weber, Y. Mao, S. D. Chang, H. P. Ding, P. J. Poole, P. J. Barrios, D. Poitras, S. Janz and M. O'Sullivan, "High performance inas/inp quantum dot 34.462-ghz c-band coherent comb laser module," *Opt. Express* **26**, 2160–2167 (2018).
3. J. Duan, H. Huang, Z. G. Lu, P. J. Poole, C. Wang and F. Grillot, "Narrow spectral linewidth in inas/inp quantum dot distributed feedback lasers," *Appl. Phys. Lett.* **112** (2018).
4. G. L. Wojcik, D. Yin, A. R. Kovsh, A. E. Gubenko, I. L. Krestnikov, S. S. Mikhlin, D. A. Livshits, D. A. Fattal, M. Fiorentino and R. G. Beausoleil, "A single comb laser source for short reach wdm interconnects," *Proc* **7230** (2009).
5. J. Duan, H. Huang, B. Dong, D. Jung, J. C. Norman, J. E. Bowers and F. Grillot, "1.3- $\mu\text{m}$  reflection insensitive inas/gaas quantum dot lasers directly grown on silicon," *IEEE Photonics Technol. Lett.* **31** (2019).
6. A. Liu, T. Komljenovic, M. Davenport, A. Gossard and J. Bowers, "Reflection sensitivity of 1.3  $\mu\text{m}$  quantum dot lasers epitaxially grown on silicon," *Opt. Express* **25**, 9535 (2017).
7. T. Kageyama, K. Nishi, M. Yamaguchi, R. Mochida, Y. Maeda, K. Takemasa, Y. Tanaka, T. Yamamoto, M. Sugawara and Y. Arakawa, "Extremely high temperature (220 °C) continuous-wave operation of 1300-nm-range quantum-dot lasers," *CLEO-Europe* (2011).
8. G. Kurczveil, M. A. Seyed, D. Liang, M. Fiorentino and R. G. Beausoleil, "Error-free operation in a hybrid-silicon quantum dot comb laser," *IEEE Photonics Technol. Lett.* **30** (2018).
9. V. R. Supradeepa and A. M. Weiner, "Bandwidth scaling and spectral flatness enhancement of optical frequency combs from phase-modulated continuous-wave lasers using cascaded four-wave mixing," *Opt. Lett.* **37** (2012).
10. Z.G. Lu, J.R. Liu, P.J. Poole, S. Raymond, P.J. Barrios, D. Poitras, G. Pakulski, P. Grant and D. Roy-Guay, "An I-band monolithic inas/inp quantum dot mode-locked laser with femtosecond pulses," *Opt. Express* **17** (2009).
11. M. Yu, Y. Okawachi, A. G. Griffith, M. Lipson and A. L. Gaeta, "Mode-locked mid-infrared frequency combs in a silicon microresonator," *Optica* **3** (2016).
12. E. Sooudi, C. de Dios, J. G. McInerney, G. Huyet, F. Lelarge, K. Merghem, R. Rosales, A. Martinez, A. Ramdane and S. P. Hegarty, "A novel scheme for two-level stabilization of semiconductor mode-locked lasers using simultaneous optical injection and optical feedback," *IEEE J. Sel. Top. Quantum Electron.* **19** (2013).
13. E. Prior, C. De Dios, R. Criado, M. Ortsiefer, P. Meissner and P. Acedo, "Dynamics of dual-polarization vcsel-based optical frequency combs under optical injection locking," *Opt. Lett.* **41** (2016).
14. F. Grillot, B. Dagens, J. G. Provost, H. Su and L. F. Lester, "Gain compression and above-threshold linewidth enhancement factor in 1.3  $\mu\text{m}$  inas-gaas quantum dot lasers," *IEEE J. Quantum Electron.* **44**, 946 (2008).
15. E. K. Lau, L. J. Wong and M. C. Wu, "Enhanced modulation characteristics of optical injection-locked lasers: A tutorial," *IEEE J. Sel. Top. Quantum Electron.* **15** (2009).
16. N. A. Naderi, M. Pochet, F. Grillot, N. B. Terry, V. Kovanis and L. F. Lester, "Modeling the injection-locked behavior of a quantum dash semiconductor laser," *IEEE J. Sel. Top. Quantum Electron.* **15**, 563–571 (2009).
17. J. Jignesh, A. Lowery and B. Corcoran, "Inter-channel nonlinear phase noise compensation using optical injection locking," *Opt. Express* **26** (2018).
18. S. Liu, X. Wu, D. Jung, J. C. Norman, M. J. Kennedy, H. K. Tsang, A. C. Gossard and J. E. Bowers, "High-channel-count 20 GHz passively mode-locked quantum dot laser directly grown on Si with 4.1 Tbit/s transmission capacity," *Optica* **6**, 128–134 (2019).
19. T. Akiyama, H. Kuwatsuka, N. Hatori, Y. Nakata, H. Ebe and M. Sugawara, "Symmetric highly efficient 0 db wavelength conversion based on four-wave mixing in quantum dot optical amplifiers," *IEEE Photonics Technol. Lett.* **14**, 1139 (2002).
20. Govind P. Agrawal, "Population pulsations and nondegenerate four-wave mixing in semiconductor lasers and amplifiers," *J. Opt. Soc. Am. B* **5**, 147–159 (1988).
21. M. De Cea, A. H. Atabaki and R. J. Ram, "Power handling of silicon microring modulators," *Opt. Express* **27**, 24274–24285 (2019).
22. M. Osinski and J. Buus, "Linewidth broadening factor in semiconductor lasers: An overview," *IEEE J. Quantum Electron.* **23**, 9 (1987).
23. F. Cappelli, G. Villares, S. Riedi and J. Faist, "Intrinsic linewidth of quantum cascade laser frequency combs," *Optica* **2**, 836–840 (2015).
24. M. Heuck, S. Blaaberg and J. Mørk, "Theory of passively mode-locked photonic crystal semiconductor lasers," *Opt. Express* **18** (2010).
25. F. Grillot, K. Veselinov, M. Gioannini, I. Montrosset, J. Even, R. Piron, E. Homeyer and S. Loualich, "Spectral analysis of 1.55- $\mu\text{m}$  inas–inp(113)b quantum-dot lasers based on a multipopulation rate equations mode," *IEEE J. Quantum Electron.* **45**, 872–878 (2009).